Enhanced delivery of galanin conjugates to the brain through bioengineering of the anti-transferrin receptor antibody OX26

Thom, George; Burrell, Matthew; Haqqani, Arsalan S.; Yogi, Alvaro; Lessard, Etienne; Brunette, Eric; Delany, Christie; Baumann, Ewa; Callaghan, Deborah; Rodrigo, Natalia; Webster, Carl I.; Stanimirovic, Danica B.

Publisher's version / Version de l'éditeur:
https://doi.org/10.1021/acs.molpharmaceut.7b00937
Molecular Pharmaceutics, 2018-02-27

molecular pharmaceutics

Subscriber access provided by National Research Council Canada

Article

Enhanced delivery of galanin conjugates to the brain through bioengineering of the anti-transferrin receptor antibody OX26

George Thom, Matthew Burrell, Arsalan S. Haqqani, Alvaro Yogi, Etienne Lessard, Eric Brunette, Christie Delany, Ewa Baumann, Deborah Callaghan, Natalia Rodrigo, Carl I. Webster, and Danica B. Stanimirovic

Mol. Pharmaceutics, **Just Accepted Manuscript** • DOI: 10.1021/acs.molpharmaceut.7b00937 • Publication Date (Web): 27 Feb 2018

ACS Publications

Molecular Pharmaceutics is published by the American Chemical Society. 1155 Sixteenth Street N.W., Washington, DC 20036

Enhanced delivery of galanin conjugates to the brain through bioengineering of the anti-transferrin receptor antibody OX26

George Thom[1], Matthew Burrell[1], Arsalan S Haqqani[2], Alvaro Yogi[2], Etienne Lessard[2], Eric Brunette[2], Christie Delaney[2], Ewa Baumann[2], Deborah Callaghan[2], Natalia Rodrigo[1], Carl I Webster[1*], Danica B Stanimirovic[2]

Affiliations:

[1]Antibody Discovery and Protein Engineering, MedImmune, Milstein Building, Granta Park. Cambridge. CB21 6GH. UK

[2]National Research Council of Canada, Human Health Therapeutics Portfolio, Ottawa, ON K1A0R6

Corresponding Author:

* Carl Webster, MedImmune, Milstein Building, Granta Park, Cambridge. CB21 6GH. United Kingdom email:websterc@medimmune.com, Tel: + 44 2037496652. Fax: +44 1223 471472

Abstract

The blood-brain barrier (BBB) is a formidable obstacle for brain delivery of therapeutic antibodies. However, antibodies against the transferrin receptor (TfR), enriched in brain endothelial cells, have been developed as delivery carriers of therapeutic cargos into the brain via a receptor-mediated transcytosis pathway. *In vitro* and *in vivo* studies demonstrated that either a low-affinity or mono-valent binding of these antibodies to the TfR improves their release on the abluminal side of the BBB and target engagement in brain parenchyma. However, these studies have been performed with mouse-selective TfR antibodies that recognize different TfR epitopes and have varied binding characteristics. In this study, we evaluated serum pharmacokinetics, brain and CSF exposure of the rat TfR-binding antibody OX26 affinity variants, having K_ds of 5 nM, 76 nM, 108 nM and 174 nM; all binding the same epitope in bi-valent format. Pharmacodynamic responses were tested in Hargreaves chronic pain model after conjugation of OX26 affinity variants with the analgesic and anti-epileptic peptide, galanin. OX26 variants with affinities of 76 nM and 108 nM showed enhanced brain and CSF exposure and higher potency in Hargreaves model, compared to a 5 nM affinity variant; lowering affinity to 174 nM resulted in prolonged serum pharmacokinetics, but reduced brain and CSF exposure. The study demonstrates that binding affinity optimization of TfR-binding antibodies could improve their brain and CSF exposure even in the absence of mono-valent TfR engagement.

Key words: blood-brain barrier; transferrin receptor antibody; affinity optimization; pharmacokinetics; brain exposure; inflammatory pain

Introduction

Antibodies have emerged as a class of therapeutics that can be engineered to demonstrate an exquisite selectivity, specificity and affinity, or to engage multiple targets, and therefore have significant advantages over synthetic molecules for some therapeutic indications.[1] The blood brain barrier (BBB), formed by the tight-junction sealed brain endothelial cells, presents a major impediment for developing efficacious antibody-based therapeutics for central nervous system (CNS) diseases.[2,3] However, the delivery of CNS-targeting antibodies across the BBB can be achieved by 'coupling' them with carrier molecules that engage the BBB receptor-mediated transcytosis (RMT) process.[2,4,5] The most studied receptor undergoing RMT is transferrin receptor (TfR). This receptor is enriched in brain endothelial cells compared to peripheral endothelium,[6,7] but it is also abundant in blood cells (bone marrow; reticulocytes) and lung.[8] The trafficking of transferrin and anti-transferrin receptor antibodies across the BBB by RMT has been demonstrated *in vitro* and *in vivo*.[9,10]

The attributes of anti-TfR antibodies studied in relation to their ability to efficiently transcytose across the BBB include affinity,[11] valency,[12] and pH sensitivity of receptor binding.[13] Notably, it has been shown that antibodies displaying high-affinity binding to TfR preferentially accumulate in brain vessels without efficient release on the abluminal side of brain endothelium.[11,14–17] Lowering their affinity facilitated their sorting into early endosomes,[18] improved their transcytosis and increased their levels in the brain parenchyma.[11,19] The comparisons of TfR engagement with bi-valent or monovalent TfR antibodies revealed that a monovalent format achieved improved transcytosis across the BBB, regardless of affinity,[12] whereas a high-affinity bi-valent antibody was destined to degradation in brain endothelial lysosomes.[12] A pH-sensitive bi-valent TfR antibody, with lower binding affinity at the acidic pH found in endocytic compartments, also demonstrated improved BBB transcytosis *in vitro.*[13] Recent study also showed that the mouse anti-TfR antibody 8D3 bioengineered to reduce Kd

from 1.2 nM to 130 nM resulted in a 44-fold increase in total brain and spinal cord exposure [19]. The various studies above examined TfR antibodies that bound different epitopes on TfR and it is therefore difficult to extend their findings into generic principles that govern TfR-anti-TfR – mediated transcytosis across the BBB.

In this study we developed affinity variants of the known rat TfR-specific antibody OX26 and evaluated their pharmacokinetics, brain and CSF exposure to examine whether affinity modulation/optimization of bi-valent anti-TfR antibodies binding the same receptor epitope is sufficient to improve their brain and CSF exposure and to engage central target. The data demonstrate that OX26 with affinities in the 76-108 nM range produced a significantly higher CNS exposure, neuronal cell engagement and higher potency in pharmacodynamics chronic pain model, compared to either high affinity (5 nM) or low affinity (174 nM) variants binding the same epitope.

Experimental Section

Protein expression and purification

DNA encoding the V_H and V_L of the mouse anti-rat TfR antibody OX26 was synthesized by Life Technologies (Carlsbad, CA) and cloned into expression vectors containing the appropriate light or heavy chain constant regions.[20] Single alanine substitutions were introduced into the V_H complementarity determining region 1 (CDR1) and V_H or V_L CDR3 regions of OX26 by site-directed mutagenesis. Unless otherwise stated, OX26 variants were expressed as chimeric human IgG1 molecules with the S239D/A330L/I332E triple mutation (IgG1 TM)[21] (Supplementary Table 1). Antibodies were expressed in transiently transfected Chinese hamster ovary (CHO) cells in serum-free media as described previously.[22] Cultures were maintained in a humidified incubator at 37°C, 5% CO_2 for 14 days after which the medium

was harvested. Antibodies were purified from cell culture media using protein A affinity chromatography followed by size exclusion chromatography. The concentration of IgG was determined by A_{280} using an extinction coefficient based on the amino acid sequence of the IgG.[23]

The control antibody, NiP228, a full IgG binding to the hapten nitrophenol, of identical isotype to the test antibodies, was produced and purified using the same methods. In some experiments, fusion of A20.1, a camelid single-domain antibody against *C. difficile* toxin B, and the mouse Fc (A20.1mFc), also expressed in CHO cells, was used for normalization of responses across experimental groups.

To allow site-specific conjugation of bio-active drug molecules, antibodies were generated containing three cysteine residues introduced into the solvent exposed surface of the Fc region.

The extracellular domain (L101 to F761) of rTfR was expressed with flag and 10His tags at its C-terminus. Expression was performed in CHO cells as described above and the protein was purified by Ni-affinity and size exclusion chromatography.

Affinity determination

Affinity of OX26 variants for rTfR was determined using an assay in which binding was monitored using the Octet RED384 System (Pall ForteBio LLC, Menlo Park, CA). Human IgG1 TM molecules were immobilized onto anti-human Fc capture biosensors at 10 µg/mL in Octet kinetics buffer (PBS containing1 mg/mL BSA and 0.01% Tween-20). Association of rTfR was monitored at receptor concentrations of 1-2000 nM for 300 seconds after which dissociation was monitored for 300 seconds. Binding curves were fit with a 1:1 binding model to generate kinetic parameters using Octet Data Analysis Software.

Animals

All studies to measure antibody exposure in the periphery and brain were performed at Quotient Biosciences (Newmarket, UK) in male Sprague-Dawley rats.

CSF collections and Hargreaves model of inflammatory pain were performed at the National Research Council (NRC) of Canada. All animal procedures were approved by the NRC's Animal Care Committee and were in compliance with the Canadian Council of Animal Care guidelines. All animals were purchased from Charles River Laboratories International, Inc. (Wilmington, MA, USA). Animals were housed in groups of three in a 12-hour light/dark cycle at a temperature of 24°C, a relative humidity of 50 ± 5%, and were allowed free access to food and water. Male Wistar rats aged 8-10 weeks (weight range, 230–250 g) were used in these studies.

Blood/brain pharmacokinetics

Five groups of male Sprague-Dawley rats were intravenously injected with each of the anti-rTfR antibodies or control IgG at 20 mg/kg. Intravenous doses were administered into a tail vein at a constant dose volume of 10 ml/kg. Antibodies were supplied in D-PBS (Sigma). Following dosing, three blood plasma samples were collected into individual Li-Heparin containers from each of six animals per time point. Plasma samples were taken at the following times post-dose for all dose groups – 10 minutes, 1, 2, 4, 6, 8, 24, 48 and 72 hours.

The first and second blood samples from each animal were collected from the lateral tail vein (*ca* 400 µl) into a Li-Hep microtainer (BD Diagnostic Systems), while the final sample (*ca* 5 ml) was collected by cardiac puncture under isoflurane anaesthesia into a Li-hep container (BD Diagnostic Systems). Following collection, blood samples were centrifuged at 10,000 x g for 2

minutes at 4°C and the resultant plasma drawn off. Terminal blood samples were centrifuged at 2500 x g for 10 minutes at 4°C. Plasma samples were flash frozen on dry ice for subsequent analysis. After final blood collection each animal remained under anaesthesia and had the chest cavity opened to allow access to the heart. A 50 ml syringe with attached 16G needle pre-loaded with PBS was inserted into the left ventricle. The right ventricle was then carefully cut prior to gentle perfusion until the extremities (paws and ears) appeared white. The animal was considered fully perfused after 50 ml D-PBS had been administered. The cranium of each animal was opened and the brain fully removed and divided into two hemispheres. One hemisphere was snap frozen in liquid nitrogen, and the second hemisphere was weighed and homogenized as detailed below.

Brain hemispheres were individually homogenized in 5 volumes of ice-cold PBS containing 1% NP-40 and Complete® protease inhibitor cocktail tablets (Roche Diagnostics). Homogenization was achieved in a 10 ml Potter-Elvehjem mortar type glass homogenizer with PTFE pestle, using 2x10 clockwise strokes with 5 sec rest time. Homogenates were transferred to LoBind tubes (Eppendorf) and rotated at 4°C for 1 hour before centrifuging in a chilled bench-top centrifuge at 13,000 g for 20 minutes to remove cell debris, including capillaries. The resulting capillary free supernatant was carefully removed for brain antibody measurement as described.[19]

Determination of antibody concentration in plasma and brain homogenate

Antibody concentrations in rat plasma and brain samples were measured using a method to detect human IgG assay on the MesoScale Discovery (MSD) assay platform. The MSD employs a plate-based sandwich immunoassay format where anti-human IgG capture antibody binds calibrator or samples. Plates were blocked with PBS and 3% membrane blocking

agent (GE Healthcare) for 1 hour at 25°C. A standard 12 point concentration curve for each antibody (control IgG and anti-TfR variants) was used as an internal standard on each MSD plate to quantify respective antibody concentrations from plasma and brain samples. Plates were washed with PBS and 0.1% Tween 20 with a microplate washer (Bio-Tek Instruments Inc.). All analyte samples and standards were diluted in PBS containing 1% membrane blocking agent and 25 µl was added per well of the plate and incubated for 2 hours at 25°C. Antibody from the standard control wells and analyte antibody samples were detected via a specific SULFO-TAG labelled anti-human IgG detection antibody (that recognizes a different region of the human IgG) which emits light upon electrochemical stimulation. The plates were measured immediately on a MSD MesoSector S600. Analyte antibody concentrations were determined from the standard curve with a four-parameter nonlinear regression program.

Analyses of Pharmacokinetic Parameters

Serum and brain concentration-time profiles were analyzed using WinNonlin software (Version 7.0, Pharsight Corporation, Mountain View, CA, USA).

Plasma concentration-time data for $OX26_{76}$, $OX26_{108}$, $OX26_{174}$ and NiP228 group were analyzed using naive pooled data and a two-compartment model with IV bolus input, first-order elimination, and macro-rate constants to estimate the following pharmacokinetic parameters: Volume of distribution of the central compartment (V_1) and of the peripheral compartment (V_2), Clearance (CL), Inter-compartmental Clearance (CL_D) and overall elimination half-life ($t_{1/2\beta}$). For $OX26_5$, plasma concentration-time profile was analyzed with a one-compartment model to estimate the following parameters: Clearance, Volume of distribution and terminal half-life. Overall, goodness of fit was based upon the predicted estimate and percent coefficient of

variation (% CV) for primary and secondary parameters, as well as inspection of residual plots between observed and predicted concentration-time data.

To compare brain uptake kinetics of the different variants, an empirical model incorporating serum pharmacokinetics parameters combined with brain uptake clearance from serum central compartment ($CL_{up,brain}$) and clearance from the brain back to serum central compartment ($CL_{out,brain}$) was derived. In this model, serum pharmacokinetic parameters were fixed to values *a priori* determined from the serum pharmacokinetic analysis and brain volume was fixed to a physiological value of 8.14 mL/kg that represents the typical total brain volume in rat.[24] The secondary parameter, area under the curve (AUC) was estimated from both predicted serum and brain concentration-time curves and was used to calculate (AUC_{Brain}/AUC_{Serum}) X 100. Predicted maximum concentration in brain from the model ($C_{max,brain}$) was also reported.

CSF pharmacokinetics

In these experiments, a combination of control and 'test' antibodies was administered i.v. into tail vein in equimolar doses. CSF sample collections were made from cisterna magna by needle puncture up to five times over 96 hours. For sample collection rats were briefly and lightly anesthetized with 3% isoflurane, placed in a stereotaxic frame with the head rotated downward at a 45° angle. A 2- cm midline incision between the ears beginning at the occipital crest was made and muscles separated to expose dura mater covering cisternae magna. A 27G butterfly needle (QiuckMedical, Cat# SV27EL) with tubing attached to 1 ml syringe was used to puncture dura and aspirate the ~20 μl of CSF. The CSF is then transferred into the sample glass vial (Waters, Cat#186000384c) and placed in −80°C freezer until further analysis.

Blood samples were collected from the tail vein in a commercially available tube (BD microtainer, Cat# 365956). After clotting at room temperature for 15-30 minutes, the clot was removed by centrifuging at 1100 rcf (3422rpm) for 10 minutes; serum is then transferred into a clean glass vial (Waters, Cat#186000384c), frozen on dry ice and then stored at -80°C until further analysis. At the end of collection, rats were sacrificed by cardiac puncture.

CSF and serum levels of antibodies were determined using multiplex SRM analytical method as described in following sections.

Mass spectrometry methods

OX26 affinity variants and control antibody levels in blood and CSF samples were quantified using targeted nanoLC MS/MS.

Sample preparation for Mass spectrometry

Filter-aided sample preparation method was used to prepare the samples for mass spectrometry.[25] Briefly, each sample was reduced in 3.5% SDS, 100 mM Tris-HCl, 100 mM DTT by boiling for 10 minutes. A 6.6-volume of Urea solution (8M Urea, 100 mM Tris-HCl, pH 8.5) was added to the sample and they were transferred to pre-wetted Amicon-30 spin columns (Millipore, Billerica, MA, USA) and spun as per manufacturer's instructions. The proteins were washed three times with the Urea solution, alkylated (10 mM iodoacetamide, 30-60 minutes at room temperature in dark), and then washed four times with the Urea solution and four times with 50 mM ammonium bicarbonate. The samples were digested using trypsin at 37°C and the peptides were eluted for SRM analysis.

Mass spectrometry and selected reaction monitoring (SRM)

All samples were analyzed on a reversed-phase nanoAcquity UPLC (Waters, Milford, MA) coupled to LTQ XL ETD or LTQ Orbitrap ETD mass spectrometer (ThermoFisher, Waltham, MA). The analysis involved injection and loading of the desired aliquot of the sample onto a 300 µm I.D. × 0.5 mm 3µm PepMaps® C18 trap (ThermoFisher) followed by eluting onto a 100 µm I.D. × 10 cm 1.7 µm BEH130C18 nanoLC column (Waters) using a gradient from 0% - 20% acetonitrile (in 0.1% formic) in 1 minute, 20% - 46% in 60 minutes, and 46% - 95% in 1 minute at a flow rate of 400 nL/min. The eluting peptides were ionized into the mass spectrometer by electrospray ionization (ESI) for MS/MS using collision induced dissociation (CID) for fragmentation of the peptide ions. Data was acquired on ions with mass/charge (m/z) values between 400 and 2,000 with 1.0 second scan duration and 0.1 second interscan interval. To develop the SRM assay for proteins, samples (pure antibodies and endosome fractions) were first analyzed by nanoLC-MS/MS using data-dependent acquisition to identify ionizible peptides of antibodies used (Supplementary Table 2). Once these spectra were validated as unique signatures, multiplexed methods of these peptides were created for SRM analysis to allowed targeted quantification of the proteins in the fraction. SRM analyses were carried out as previously described.[26] For ILIS-based quantification, isotopically heavy versions of the peptides were synthesized (New England Peptide LLC, Gardner, MA) containing heavy C-terminus K (+8 Da). SRM analyses were carried out as previously described.[26]

The blood contamination of CSF samples was evaluated by ‘in-reaction’ monitoring of albumin levels using a nanoLC-SRM method and albumin signatures as described previously [26]. A CSF/serum ratio of albumin higher than 0.07% was considered blood contamination and these CSF samples were excluded from further analyses.

Serum/CSF pharmacokinetic parameters

Mean serum and CSF concentration values were used to generate a composite pharmacokinetic profile. A non-compartmental approach consistent with the intravenous route of administration and using the linear/log trapezoidal method was employed to estimate the area under the curve (AUC) of the serum concentration vs time and CSF concentration vs time. For both serum and CSF, the area under concentration versus time curve from the start of dose administration to the last observed quantifiable (AUC_{0-96}) was estimated. Estimation of average concentration ratios for AUC_{0-96} is reported as (AUC_{CSF}/AUC_{Serum}) x 100.

Detection of antibodies in brain sections by immunofluorescence

After iv administration of antibodies (7 mg/kg iv; 4 hours), rat brains were perfused with 20 ml of 0.9% saline supplemented with 1EU/ml Heparin (Organon, Toronto, ON) at 2 ml/minute. Brains were removed, cut in four pieces and fixed in 10% neutral buffered formalin overnight at room temperature (RT), then rinsed and incubated in 30% sucrose solution at 4^{o}C for 48 hours. Pieces were then rinsed in PBS and frozen in OCT in Isopentane (Cat# M23631, Sigma) over dry ice.

A 25 μM-thick free floating sections, cut using cryostat and stored in physiological buffered saline (PBS) (Cat# 311-012-Cl, Wisent) containing 0.5% NaN_3 (Cat# S2002, Sigma), were mounted on a Superfrost slides (Cat#12-550-123, Fisher Scientific), dried for 2 hour at RT, and then incubated with 20% normal goat serum (NGS) containing 0.3% TritonX-100 in PBS for 1hour followed by biotinylated goat anti-human IgG (Cat#BA3080, Vector Labs) diluted 1:50 in 10% normal goat serum (NGS)/PBS at 4^{o}C overnight. After washing 3 times in PBS, slides were exposed to Streptavidin-cy3 (Cat# 016-160-084, Jackson ImmunoResearch) diluted

1:1000 in PBS for 1 hour at RT. After washing 3 times in PBS, slides were incubated in mouse anti-NeuN (Cat#MAB377, Millipore) diluted 1:300 in 10% NGS/PBS for 2 hour at RT, and after washing, in goat anti-mouse Alexa 488 (Cat# A11001, Invitrogen) diluted 1:500 in PBS for additional 1 hour at RT. After washing, cell nuclei were counter-stained with Hoechst (Cat#H3570, Invitrogen)- 1:10000 of 10mg/mL stock in PBS for 15 min at RT and slides cover slipped in Dako fluorescent mounting medium (Dako, Burlington, ON). Images were captured with Olympus 1X81 Fluorescent Microscope (Olympus, Richmond Hill, ON) using 10X and 60X objectives.

Pharmacodynamic read-out using neuropeptide cargo

Antibody conjugation to galanin

The neuropeptide galanin, YPSKPDNPGEDAPAEDMARYYSALRHYINLITRQRY, was chemically synthesised by Bachem (Bubendorf, Switzerland) with a maleimide group attached to the C-terminus via the ε-amino group of an additional lysine residue to allow conjugation to thiol group of engineered cysteine residues on the Fc region of human antibodies.[27] Briefly, to achieve site specific peptide conjugation, cysteine engineered OX26 variant antibodies, were first reduced with 40 molar equivalents of Tris-(2-carboxyethyl)-phosphine (TCEP) in PBS pH7.2, 1mM EDTA (Ethylenediaminetetraacetic acid) for 3 hours at room temperature. Following buffer exchange to remove TCEP, 20 molar equivalents of dehydroascorbic acid (dhAA) were added for 4 hours at room temperature. The resulting solution was filtered through a 0.2 uM syringe filter and 7.5 molar equivalent of the galanin peptide was then added followed by incubation at room temperature for 1 hour and subsequently at 4°C overnight. The reaction was quenched by the addition of 4 equivalents of N-acetyl cysteine. Labelled antibody was separated from free peptide by size-exclusion chromatography over a Superdex 200 26/600

column in PBS. The peptide to antibody ratio was estimated as described in Thompson et al.[27] Briefly, the extent of conjugation was determined by measuring the mass shift between unlabelled and labelled antibody by matrix-associated laser desorption/ionization time-of-flight mass spectrometry performed on a Shimadzu Biotech Axima Assurance mass spectrometer. Galanin conjugated antibodies had an average drug-antibody ratio (DAR) of 4-5. Endotoxin levels were measured using the Charles River Endosafe-PTS system and all antibodies used for *in vivo* studies contained <1 EU/mg.

Hargreaves model of inflammatory pain (thermal hyperalgesia)

Rats aged 6-8 weeks (weight range, 230–250 g) were used for intravenous (iv) administrations of various antibodies and evaluation of their efficacy in the Hargreaves model of inflammatory pain.[28] This model measures the paw withdrawal latency (PWL) in response to the application of a radiant stimulus onto the plantar surface of the hind paws using the plantar Analgesia Meter equipment for paw stimulation (IITC Life Science, Woodland Hills, CA) exactly as described in Farrington et al.[29] The time taken by the animal to respond by licking or flicking its paw is interpreted as positive nociceptive behavior. A cut-off time (20 seconds) is established at the end of which the heat source shuts off automatically to avoid tissue damage**.**

All animals were allowed to acclimatize to the facility and staff prior to the beginning of experiments. On day 1, PWL was measured and chronic inflammatory pain was induced by injecting a low volume (100 µl) of complete Freund's adjuvant (CFA; heat-killed *M.tuberculosis* [Sigma, St. Louis, MO] suspended in oil:saline 1:1 emulsion) into the plantar surface of the right hind paw. On day 3 after CFA injection, baseline PWL of right and left hind paws were measured to confirm the development of inflammatory hyperalgesia (PWL of inflamed paw dropping from 20s to ~5s); animals with PWL time above 7s were excluded from further studes. Antibodies were then administered by iv route through the tail vein. Experimenter performing pain experiments was blinded to the content of injectable compounds. Reversal of CFA-

induced hyperalgesia was measured for up to 240 minutes. Once PWL returned to baseline values, a single and terminal sample of CSF and serum was collected as previously described and animals euthanized under deep anesthesia.

Fitted curves of the PWL were used to determine maximum response (percent of reversal of hyperalgesia at the peak response), time to maximum response, duration of the hyperalgesia inhibition and pharmacological exposure, defined as AUC of hyperalgesia inhibitory response. Response was defined as paw withdrawal latencies values that were statistically different from baseline values. AUC was calculated by the trapezoidal method and was used to derive percentage of reversal using the formula: % of reversal $= [(AUC_{molecule} - AUC_{inflamed\ paw})/(AUC_{normal\ paw} - AUC_{inflamed\ paw})] \times 100$, where $AUC_{inflamed\ paw}$ and $AUC_{normal\ paw}$ are the values obtained from the group injected with the vehicle (PBS) and the left paw, respectively.

The statistical significance used to compare differences between treatments in behavioral experiments was determined by One-way analysis of variance (ANOVA), followed by Tukey's test. Differences were considered statistically significant at $P < 0.05$.

Results

OX26 Variants Binding to Transferrin Receptor

To generate a panel of OX26 variants with reduced affinity for rTfR, single alanine substitutions were introduced into HCDR1, HCDR3 or LCDR3 and resulting mutants were characterized using an Octet binding assay. An affinity of 5 nM was measured for wild-type OX26 (Table 1). The majority of alanine substitutions had little or no effect on affinity of the antibody. However, a number of variants were identified that had between 5- and 70-fold

reduced affinities compared to wild-type OX26. For example, the single alanine substitutions HCDR1 W33A, LCDR3 W96A and HCDR3 F99A resulted in variant antibodies with K_D values of 76, 108 and 174 nM, respectively (Table 1). These reductions in affinity were driven largely by increases in off-rate. No appreciable reductions in binding affinities were measured at acidic pH of 5.6 (data not shown). Binding studies using Mirrorball® high-sensitivity microplate cytometry assays confirmed strong binding of $OX26_5$, moderate binding of $OX26_{76}$ and $OX26_{108}$ and virtually no binding of $OX26_{174}$ to rat brain endothelial cell line, SV-ARBEC (Supplementary Figure 1). Since previous work has demonstrated that affinity in the range of 50-600 nM results in high brain uptake of antibodies that bind mouse TfR,[11] the three variants above were selected for further *in vitro* characterization and measurement of brain exposure and ability to deliver a drug cargo to the CNS *in vivo*.

The HCDR1 W33A, LCDR3 W96A and HCDR3 F99A mutants will be referred to herein as $OX26_{76}$, $OX26_{108}$ and $OX26_{174}$ on the basis of their respective affinities.

Plasma Pharmacokinetics and Brain Exposure of OX26 Variants

Plasma and brain levels of OX26 variants and NiP228 were measured at different time points after iv dosing of 20 mg/kg (130 nmol/kg). Dosing concentration was chosen to enable reliable brain tissue detection of non-crossing control antibodies by ELISA.

Figure 1A and Table 2 show both observed and predicted serum concentration and brain concentration-time profiles for OX26 variants and NiP228. Whereas $OX26_5$ has short serum $t_{1/2}$ of 6 h (monoexponential decay), the medium affinity $OX26_{76}$ showed biphasic decay, with clear distribution and elimination phases and terminal serum $t_{1/2}$ of around 30 h. Serum $t_{1/2}$ of $OX26_{108}$ and $OX26_{174}$ was essentially identical (~50 h) to that of control antibody NiP228.

AUC_{Brain} / AUC_{Serum} ratio was observed with $OX26_{76}$ (1.84%), followed by $OX26_{108}$ (0.47%) and $OX26_{174}$ (0.28%). Both $OX26_5$ and NiP228 (shown in Figure 1A insets with different scale) had very low ratios. $C_{max,Brain}$ for all variants was observed at 24 h after administration; and was similar for $OX26_{76}$ and $OX26_{108}$ (3.35 and 3.10 nM, respectively), compared to 1.2 nM for $OX26_{174}$ (Figure 1A, Table 2). Relative comparisons of $CL_{up,brain}$ results in similar ranking for brain uptake to that observed from analysis of AUC_{Brain} / AUC_{Serum} ratios (Table 2). The brain clearance rates ($CL_{out,brain}$) of OX26 affinity variants (with the exception of $OX26_5$, where low brain exposure made it difficult to accurately evaluate brain clearance) showed inverse linear correlation (r=0.94) with their binding affinity. Overall, the data suggested that the high brain exposure achieved with $OX26_{76}$ and $OX26_{108}$ resulted from a combination of improved pharmacokinetics (compared to $OX26_5$) and facilitated transport across the BBB. However, lower affinity $OX26_{174}$ demonstrated reduced brain exposure, despite further improved plasma pharmacokinetics, likely because the affinity was below optimal for sufficient engagement of transcytosis via TfR.

CSF Levels of OX26 Variants

To evaluate CSF levels of OX26 affinity variants, we used a sensitive mass spectroscopy SRM method applicable for very small sample volumes of CSF obtained by repeated collections over 96 h, described in detail previously.[29,30] The method allows for simultaneous (multiplexed) measurements of co-injected control antibody, as well as albumin levels in CSF to control for potential blood contamination. An OX26 variant or NiP228 and control antibody A20.1mFc, used for normalization across experiments and to ensure that the BBB is intact in each animal, were co-injected into tail vein at equimolar (30 nmol/kg) doses.

The CSF levels measured for A20.1mFc in all experiments were below 0.7 nM at 6 h and 24 h, and declined to <0.05 nM at subsequent time points (48-96h) (Figure 1B), giving

serum/CSF ratio over time of ~0.1%. Similar CSF levels were measured for control antibody NiP228 (Figure 1B), confirming minimal penetration of these two control molecules into CSF.

$OX26_5$, $OX26_{76}$ and $OX26_{108}$ all showed higher CSF exposure compared to either A20.1mFc or NiP-228 (Figure 1B, Table 3), whereas $OX26_{174}$ exhibited slightly, but not significantly higher CSF levels compared to control antibodies (Figure 1B, Table 3). The highest CSF levels (CSF_{max}) were obtained with $OX26_{76}$ (3.1 nM); closely followed by $OX26_{108}$. The CSF_{max} values for these 2 variants were 1.6 to 1.8 -fold higher, respectively, from those of $OX26_5$ and 4- to 6-fold higher, respectively, from CSF_{max} values of $OX26_{174}$ and NiP228. For $OX26_5$, $OX26_{76}$ and $OX26_{108}$ peak levels in CSF were between 6- and 24 hours after injection.

Localization of OX26 Variants in Brain Sections by Immunostaining

Human IgG immunoreactivity was determined by immunofluorescence staining of brain sections of animals injected iv with 30 nmol/kg of NiP228, $OX26_5$ or $OX26_{76}$ and perfused 4 hours after injections. The co-localization with neurons was evaluated by counter-staining the sections for neuron body-specific antigen NeuN.

Whereas immunoreactivity of NiP228 could not be detected (Figure 2 A1-2), sections of frontal (Figure 2C1-2) and parietal (Figure 2 D1-2) cortices of animals injected with $OX26_5$ showed a high- intensity anti-IgG immunofluorescence in brain vessels, and no positivity of neuronal cells. Sections of frontal (Figure 2E1-4) and parietal (Figure 2F1-4) cortices of animals injected with the lower affinity $OX26_{76}$ variant, in addition to anti-IgG immunoreactivity in brain vessels, also displayed multiple NeuN-positive neuronal cells bodies (indicated by stars in red-channel images). The immunopositive neurons in $OX26_{76}$-injected animals were also detected in dental gyrus, caudate-putamen, and ventral thalamus, but not in dorsal thalamus (data not shown).

Data suggest an improved abluminal release of the lower affinity TfR antibody variant $OX26_{76}$ enabling more co-localization with neurons, known to express TfR and internalize TfR antibodies.

Potency of OX26 Variant-Galanin Conjugates in Hargreaves Model *In vivo*

To evaluate the brain exposure, cysteine-engineered OX26-affinity variants were chemically cross-linked to the neuropeptide galanin and evaluated for their ability to elicit a pharmacological response. Each antibody-peptide fusion contained 4-5 molecules of galanin.

Galanin and its receptors play an important role in the transmission and modulation of nociceptive information in the brain.[31] When administered systemically, this neuropeptide has no analgesic effects since it cannot cross the BBB.[32] However, injecting galanin directly into the brain has been shown to induce analgesia in different models, including the Hargreaves model of chronic inflammatory pain.[31,33] In Supplementary Figure 2, we provide a demonstration of an exquisite analgesic potency of galanin in Hargreaves model of thermal hyperalgesia when given intracerebrovetricularly, as well as a tight barrier for the CNS entry of systemically administered galanin (MW -3.2 kD) or galanin fused to human Fc (MW - 81 kD).

OX26-affinity variants conjugated with galanin 'cargo' induced various levels of suppression of thermal hyperalgesia in the same model (Figure 3A). Paw withdrawal latency of the CFA-injected paw was significantly reduced when compared to the non-injected paw (4.72±0.16 vs 19.85±0.13) at day 3 after CFA injection.

To enable ranking of potency of different variants, the dosing of variants was initially titrated so that the maximal response falls below 100% for the best-crossing variant. Therefore, the potency among OX26 affinity variants was compared at equimolar 10 nmol/kg dose. Intravenous injection of galanin-conjugated OX26-affinity variants induced a time dependent

reversal of the hyperalgesia (Figure 3A), in contrast to galanin conjugated to NiP228. $OX26_{76}$ and $OX26_{108}$ showed higher potency in the Hargreaves model, when compared to $OX26_5$ (Figure 3A and Table 4) and $OX26_{174}$. Increasing the dose of the $OX26_5$ variant to30 nmol/kg induced a response that was similar to that observed for $OX26_{76}$ and $OX26_{108}$ at 3-fold lower dose (Table 4). The higher potency of $OX26_{76}$ and $OX26_{108}$ compared to $OX26_5$ and $OX26_{174}$ was measured as the higher percent reversal, longer duration of the response and AUC of the response (Table 4). At the end of experiments (240 minutes), serum and CSF samples were harvested from each animal to measure levels of variants (Figure 3B). CSF levels of $OX26_{76}$ and $OX26_{108}$ were higher compared to $OX26_5$, whereas CSF levels of $OX26_{174}$ were similar to those of NiP228.

Discussion

The delivery of therapeutic cargo across the BBB using anti-TfR antibodies to engage receptor-mediated transcytosis (RMT) has been demonstrated in *in vitro* and *in vivo* models.[11,12,34–36] In the current study, we demonstrated that lowering binding affinity of the rat anti-TfR antibody OX26 to a range of 76-108 nM significantly enhanced total brain levels and CSF levels compared to a high-affinity (5 nM) variant. The same lower affinity variants improved the potency of the anti-nociceptive neuropeptide galanin when chemically linked to the antibodies in the Hargreaves pain model. The study demonstrates that the affinity optimization of anti-TfR antibodies improves their brain and CSF exposure in the absence of a monovalent binding to the receptor.

Various bi-specific antibodies containing an antibody against a therapeutic target in the CNS, including Aβ[12,36] and BACE1,[11,18] coupled to an anti-TfR antibody to enable transcytosis across the BBB have shown enhanced brain penetration in rodents[11,12,19,36] and, in some cases,

in non-human primates.[37] Various formats of the anti-TfR antibody 'arm' have been fused with therapeutic antibodies, including a full IgG,[36] a heterodimerized monovalent 'half' antibody,[11] mono- or bivalent fragment antigen binding – Fab,[12] and shark single-domain antibody (VNAR).[38] Whereas several studies observed intravascular 'trapping' and minimal brain penetration of high-affinity anti-TfR antibodies specific to either mouse (8D3; Ri7)[11,15,16] or rat (OX26),[14] studies with mono-valent binding of TfR antibodies in heterodimerized bi-specific antibodies[11] or as a single Fab fragment attached to the C-terminus of the therapeutic Aβ antibody[12] or as recombinant fusion of two single-chain variable fragments (scFv) to light chains of the Aβ antibody[39] demonstrated efficient translocation across the BBB, high brain exposure and central pharmacodynamic responses. However, the interpretations of these results were divergent: while Yu et al.[11] argued that the reduced affinity of the anti-TfR antibody was essential for its ability to escape intravascular 'trapping' and to release on the abluminal side of the BBB, Niewoehner et al.[12] provided evidence that the mono-valent engagement of the TfR by the antibody led to its escape from lysosomal degradation and delivery into brain parenchyma. Neither group had fully controlled (matched) the binding affinity of anti-TfR antibodies in their mono- and bi-valent formats, leaving both explanations equally plausible. Furthermore, anti-TfR antibodies used in these studies bound distinct epitopes on the TfR, another variable that could influence the nature of TfR trafficking and recycling across the BBB. The brain exposure of systemically administered RMT-targeting antibodies depends on multiple parameters, among others the BBB abundance of RMT receptor and its recycling rates, antibody ability to bind/engage and release from RMT receptor, as well as on its peripheral pharmacokinetics and biodistribution.[40] Ideally, the BBB-carrier antibody should bind highly and selectively expressed target on brain vascular cells that is not present or is low abundant in both peripheral organs and in the brain parenchyma, so that the peripheral and brain disposition and elimination of bispecific molecules is determined predominantly by the properties of the therapeutic cargo.[40]

While TfR is relatively abundant in the BBB endothelium compared to endothelial cells from other organs,[10,39] it is also highly expressed in bone marrow, immune system and erythropoietic blood cells,[8] and lung (The Human Protein Atlas; http://www.proteinatlas.org/ENSG00000072274-TFRC/tissue) affecting distribution and pharmacokinetics of high-affinity anti-TfR antibodies. TfR is also highly expressed in the neuropil[41] influencing the brain disposition of anti-TfR antibodies in an affinity-dependent manner. The interdependence of these parameters in determining brain exposure is illustrative in the presented examples of OX26 affinity variants.

As expected and described previously,[34] $OX26_5$ displayed short and mono-exponential plasma decay with $t_{1/2}$ of 6 hours, medium affinity $OX26_{76}$ exhibited a two-component plasma pharmacokinetics with elimination (terminal) half-life around 30 h, while lower affinity $OX26_{108}$ and $OX26_{174}$ variants had a terminal plasma half-life ~50 h, similar to that of an antibody that does not bind any target in the host.

High affinity $OX26_6$ internalized into brain vessels, but was not detected co-localized with neurons . Combined with a short systemic pharmacokinetics this resulted in low brain exposure similar to that achieved with a non-BBB crossing control antibody that had a long plasma pharmacokinetics. The inability of high affinity anti-TfR antibodies to release on the abluminal side of the BBB has been substantiated in several previous studies.[11,14,17] Particularly instructive in that regard are trafficking studies using anti-TfR antibody labeled with gold nanoparticles:[17] here the antibody(8D3)-TfR complex showed a predominant sorting into late endosomes, multivesicular bodies or lysosomes of the BBB endothelium, with only a small fraction (<10%) of sorting vesicles found fused with the abluminal membrane and opening to the basal membrane. In these cases, however, the 8D3-gold nanoparticles remained attached to the abluminal membrane, suggesting an endosomal escape, but not dissociation from TfR. The improved abluminal dissociation of the anti-TfR from TfR has been achieved by lowering its

binding affinity at either regular or acidic pH.[11,13] Consistent with these findings were the observations from this study that OX26 variants with lower affinities of 76 nM and 108 nM exhibited higher total brain levels as well as detectable co-localization with neuronal bodies. Whilst the absolute quantities of antibody in the brain as determined by brain homogenization may over estimate actual brain levels, the co-localization with neuronal bodies is indicative of increased brain exposure. The immunodetection of antibodies that have externalized on the abluminal side of the BBB is enabled by their binding to parenchymal target and depends on the target abundance in the brain. Since TfR is expressed in neurons, the fraction of OX26 antibodies that release from brain endothelial cells into the brain parenchyma is 'captured' as immunoreactivity associated with neurons. Notwithstanding draw backs of the indirect immunofluorescence method used in this study, which could be affected by brain autofluorescence, a clear difference between $OX26_5$ – detected in vessels only, and $OX26_{76}$ – detected in both vessels and neurons represents the evidence that $OX26_{76}$ is released into brain parenchyma more efficiently than $OX26_5$. Further reductions in the binding affinity to 174 nM resulted in lower brain exposure, despite long serum half-life, presumably due to poorer engagement of brain vascular TfR receptor at the same dosing regimen. Prior studies with anti-TfR-enabled antibodies provided sparse information about the central disposition and elimination of anti-TfR antibodies alone or in fusions with therapeutic cargos. Since TfR is highly expressed in neurons,[42] the affinity of anti-TfR antibodies may affect their bound vs. free fraction in the brain interstitial fluid, their brain residence time, and clearance rates. In this study, the binding affinity of OX26 variants (with the exception of $OX26_5$) correlated linearly (and inversely) with the brain clearance rates ($CL_{out,brain}$). The $OX26_{76}$ variant therefore showed overall higher brain exposure (slower clearance due to central target binding) despite slightly poorer systemic pharmacokinetics compared to $OX26_{108}$. Whereas this data could not be fully explained in the absence of the measurements of these antibodies in the interstitial fluid (ISF), they underscore the importance of incorporating central (brain) target abundance in developing pharmacokinetic-

pharmacodynamic (PK-PD) models for BBB-crossing bi-specific molecules. In a prior study[30] we have shown that systemically administered high-affinity antibody against mGluR1, an abundant central target, fused to an alternative BBB carrier, displays higher brain levels in combination with lower CSF exposure compared to the BBB-fused antibody that has no central target, suggesting that the high fraction of 'bound' antibody reduces 'free' antibody available for the exchange with CSF.[43] In the case of anti-TfR antibodies, the target is highly expressed in both peripheral and central compartments, and their affinity could significantly affect not only systemic pharmacokinetics and BBB delivery, but also their central disposition (unbound fraction) and pharmacology. In this study, we have also assessed CSF levels of OX26 affinity variants. CSF levels reflect the ability of the antibody to cross the blood-cerebrospinal fluid (BCSF) barrier without crossing the BBB, a likely scenario for $OX26_5$, or to transverse both BCSF and BBB, where brain interstitial fluid (ISF) exchange with CSF contributes to further increases in CSF levels as observed for lower affinity variants $OX26_{76}$ and $OX26_{108}$.

The OX26 affinity variants chemically cross-linked with the anti-nociceptive peptide galanin were evaluated in the pharmacodynamic Hargreaves model of thermal hyperalgesia. The AUC of pharmacodynamics response showed the same ranking order of OX26 variants as it was observed by measuring their brain exposure: NiP228<$OX26_5$=$OX26_{174}$<$OX26_{108}$=$OX26_{76}$. $OX26_{76}$-Gal was 3-fold more potent than $OX26_6$-Gal. Since the inhibition of thermal hyperalgesia in Hargreaves model can be measured over ~4 hours only, due to desensitization of nociceptive receptors,[40] and since the serum pharmacokinetics over this period is similar among variants, the CSF levels at the end of pharmacodynamic experiment were measured as time-matched correlate of the pharmacodynamics response; the CSF levels of variants demonstrated a strong association with the extent of their pharmacological response. In accordance with this study, another recent study[19] demonstrated that lowering the affinity of the mouse-selective anti-TfR antibody 8D3 to a range of 60-130 nM significantly improved its ability to deliver anti-nociceptive

IL-1 receptor antagonist (IL-1RA) across the blood-brain- and blood-spinal cord barriers. The pharmacological response lasted up to 7 days in a neuropathic mechanical hypersensitivity pain model in mice. Both this study in mice and our study in rats used a bi-valent, IgG format of the species-specific TfR antibody and showed that lowering their binding affinities to ~100 nM is sufficient to improve their total brain exposure in the absence of mono-valent binding to the receptor. The notable difference between OX26 and 8D3 affinity variants used in these two studies is that OX26 affinity modulation was achieved primarily by faster dissociation rates, whereas reductions in 8D3 affinities were driven by slower association rates. While in both studies a steady-state affinity of antibodies against TfR correlated inversely with their brain exposure (within a range of affinities), the relative importance of receptor binding kinetic parameters in this process remains unclear. Prior studies on TfR antibody transcytosis across the BBB have not disclosed kinetic binding parameters of various bioengineered affinity variants. Despite this study and several others finding that the reduction in affinity of anti-TfR antibodies improves brain penetration, it cannot be ruled out that other factors such as specificity or antibody structure are playing a part in the improved brain exposure.

The majority of antibodies developed against TfR are species-selective and bind different receptor epitopes. In addition, TfR expression and abundance in brain endothelial cells is variable between species, with rodents showing higher abundance than humans.[45] Studies with TfR-BACE1 heterodimerized bi-specific antibodies also showed that human-cynomolgus monkey cross-reactive anti-TfR antibody affinity required for maximal brain exposure is different between cynomolgus monkey (37 nM) and the mouse (270 nM) genetically engineered to express human TfR ectodomain.[37] This inter-species variability is further compounded by the necessity to mitigate effector function of bi-specific antibodies to alleviate on-target TfR antibody toxicity in reticulocytes [41]. Therefore, this translational complexity of the target (TfR) including inter-species variability and pharmacokinetic and toxicity liabilities will remain serious obstacles

in the development of clinically viable brain-targeting bi-specific molecules using TfR antibodies as BBB-crossing carriers. A further interesting observation from PK-PD modeling studies with TfR-BACE1 bi-specific antibodies[42,43] is that the 'benefit' of TfR variants in improving antibody brain penetration is expected only when the antibody recognizes intermediately or highly abundant target in periphery, but will be negligible for antibodies with low abundant peripheral targets which have exquisitely long pharmacokinetic profiles. Despite the efficiency of BBB transcytosis demonstrated with affinity-optimized TfR antibodies, due to above limitation, each therapeutic application will require an extensive tailoring of molecular formats to achieve acceptable risk-benefit profiles.

Acknowledgments

The authors would like to thank Arthur Beljean for his technical help in labelling the antibodies with galanin, and the following MedImmune teams: the biologics expression team for assistance with high throughput antibody expression; early material supply for large scale antibody expression and purification; and members of the neurosciences team for invaluable discussion. The work reported in the manuscript was funded jointly by MedImmune and the National Research Council of Canada (Therapeutics beyond Brain Barriers Program).

Supplementary Materials

Cell binding data and methods for the OX26-variants binding to the rat brain endothelial line (SV-ARBEC)

Inhibition of thermal hyperalgesia induced by intravenous or intracerebroventricular administration of galanin or galanin genetically fused to human Fc.

Table illustrating the mutations in OX26 leading to the lowered affinities.

Conflict of interest statement:

All authors employed by MedImmune at the time of the work have a theoretical conflict of interest through being employed by the organisation that both funded the work and has a potential commercial interest in the findings

References

(1) Imai, K.; Takaoka, A. Comparing Antibody and Small-Molecule Therapies for Cancer. *Nat. Rev. Cancer* **2006**, *6* (9), 714–727.

(2) Pardridge, W. M. Drug and Gene Delivery to the Brain: The Vascular Route. *Neuron* **2002**, *36* (4), 555–558.

(3) Abbott, N. J.; Patabendige, A. A. K.; Dolman, D. E. M.; Yusof, S. R.; Begley, D. J. Structure and Function of the Blood-Brain Barrier. *Neurobiol. Dis.* **2010**, *37* (1), 13–25.

(4) Smith, M. W.; Gumbleton, M. Endocytosis at the Blood-Brain Barrier: From Basic Understanding to Drug Delivery Strategies. *J. Drug Target.* **2006**, *14* (4), 191–214.

(5) Lajoie, J. M.; Shusta, E. V. Targeting Receptor-Mediated Transport for Delivery of Biologics Across the Blood-Brain Barrier. *Annu. Rev. Pharmacol. Toxicol.* **2015**, *55* (1), 613–631.

(6) Jefferies, W. A.; Brandon, M. R.; Hunt, S. V; Williams, A. F.; Gatter, K. C.; Mason, D. Y. Transferrin Receptor on Endothelium of Brain Capillaries. *Nature* **1984**, *312* (5990), 162–163.

(7) Pardridge, W. M.; Eisenberg, J.; Yang, J. Human Blood-Brain Barrier Transferrin Receptor. *Metabolism* **1987**, *36* (9), 892–895.

(8) Chan, L. N.; Gerhardt, E. M. Transferrin Receptor Gene Is Hyperexpressed and Transcriptionally Regulated in Differentiating Erythroid Cells. *J. Biol. Chem.* **1992**, *267* (12), 8254–8259.

(9) Broadwell, R. D.; Baker-Cairns, B. J.; Friden, P. M.; Oliver, C.; Villegas, J. C. Transcytosis of Protein through the Mammalian Cerebral Epithelium and Endothelium. *Exp. Neurol.* **1996**, *142* (1), 47–65.

(10) Hersom, M.; Helms, H. C.; Pretzer, N.; Goldeman, C.; Jensen, A. I.; Severin, G.; Nielsen, M. S.; Holm, R.; Brodin, B. Transferrin Receptor Expression and Role in Transendothelial Transport of Transferrin in Cultured Brain Endothelial Monolayers. *Mol. Cell. Neurosci.* **2016**, *76*, 59–67.

(11) Yu, Y. J.; Zhang, Y.; Kenrick, M.; Hoyte, K.; Luk, W.; Lu, Y.; Atwal, J.; Elliott, J. M.; Prabhu, S.; Watts, R. J.; Dennis, M. S. Boosting Brain Uptake of a Therapeutic Antibody by Reducing Its Affinity for a Transcytosis Target. *Sci. Transl. Med.* **2011**, *3* (84), 84ra44.

(12) Niewoehner, J.; Bohrmann, B.; Collin, L.; Urich, E.; Sade, H.; Maier, P.; Rueger, P.; Stracke, J. O.; Lau, W.; Tissot, A. C.; Loetscher, H.; Ghosh, A.; Freskgård, P.-O. Increased Brain Penetration and Potency of a Therapeutic Antibody Using a Monovalent Molecular Shuttle. *Neuron* **2014**, *81* (1), 49–60.

(13) Sade, H.; Baumgartner, C.; Hugenmatter, A.; Moessner, E.; Freskgård, P.-O.; Niewoehner, J. A Human Blood-Brain Barrier Transcytosis Assay Reveals Antibody Transcytosis Influenced by pH-Dependent Receptor Binding. *PLoS One* **2014**, *9* (4), e96340.

(14) Moos, T.; Morgan, E. H. Restricted Transport of Anti-Transferrin Receptor Antibody (OX26) through the Blood-Brain Barrier in the Rat. *J. Neurochem.* **2001**, *79* (1), 119–129.

(15) Alata, W.; Paris-Robidas, S.; Emond, V.; Bourasset, F.; Calon, F. Brain Uptake of a Fluorescent Vector Targeting the Transferrin Receptor: A Novel Application of in Situ Brain Perfusion. *Mol. Pharm.* **2014**, *11* (1), 243–253.

(16) Manich, G.; Cabezón, I.; del Valle, J.; Duran-Vilaregut, J.; Camins, A.; Pallàs, M.; Pelegrí, C.; Vilaplana, J. Study of the Transcytosis of an Anti-Transferrin Receptor Antibody with a Fab′ Cargo across the Blood–brain Barrier in Mice. *Eur. J. Pharm. Sci.* **2013**, *49* (4), 556–564.

(17) Cabezon, I.; Manich, G.; Martin-Venegas, R.; Camins, A.; Pelegri, C.; Vilaplana, J. Trafficking of Gold Nanoparticles Coated with the 8D3 Anti-Transferrin Receptor Antibody at the Mouse Blood-Brain Barrier. *Mol. Pharm.* **2015**, *12* (11), 4137–4145.

(18) Bien-Ly, N.; Yu, Y. J.; Bumbaca, D.; Elstrott, J.; Boswell, C. A.; Zhang, Y.; Luk, W.; Lu, Y.; Dennis, M. S.; Weimer, R. M.; Chung, I.; Watts, R. J. Transferrin Receptor (TfR) Trafficking Determines Brain Uptake of TfR Antibody Affinity Variants. *J. Exp. Med.* **2014**, *211* (2), 233–244.

(19) Webster, C. I.; Hatcher, J.; Burrell, M.; Thom, G.; Thornton, P.; Gurrell, I.; Chessell, I. Enhanced Delivery of IL-1 Receptor Antagonist to the Central Nervous System as a Novel Anti–transferrin Receptor-IL-1RA Fusion Reverses Neuropathic Mechanical Hypersensitivity. *Pain* **2017**, *158* (4), 660–668.

(20) Persic, L.; Roberts, A.; Wilton, J.; Cattaneo, A.; Bradbury, A.; Hoogenboom, H. R. An Integrated Vector System for the Eukaryotic Expression of Antibodies or Their Fragments after Selection from Phage Display Libraries. *Gene* **1997**, *187* (1), 9–

18.

(21) Oganesyan, V.; Damschroder, M. M.; Leach, W.; Wu, H.; Dall'Acqua, W. F. Structural Characterization of a Mutated, ADCC-Enhanced Human Fc Fragment. *Mol. Immunol.* **2008**, *45* (7), 1872–1882.

(22) Daramola, O.; Stevenson, J.; Dean, G.; Hatton, D.; Pettman, G.; Holmes, W.; Field, R. A High-Yielding CHO Transient System: Coexpression of Genes Encoding EBNA-1 and GS Enhances Transient Protein Expression. *Biotechnol. Prog.* **2014**, *30* (1), 132–141.

(23) Pace, C. N.; Vajdos, F.; Fee, L.; Grimsley, G.; Gray, T. How to Measure and Predict the Molar Absorption Coefficient of a Protein. *Protein Sci.* **1995**, *4* (11), 2411–2423.

(24) Shah, D. K.; Betts, A. M. Towards a Platform PBPK Model to Characterize the Plasma and Tissue Disposition of Monoclonal Antibodies in Preclinical Species and Human. *J. Pharmacokinet. Pharmacodyn.* **2012**, *39* (1), 67–86.

(25) Wiśniewski, J. R.; Zougman, A.; Nagaraj, N.; Mann, M. Universal Sample Preparation Method for Proteome Analysis. *Nat. Methods* **2009**, *6* (5), 359–362.

(26) Haqqani, A. S.; Caram-Salas, N.; Ding, W.; Brunette, E.; Delaney, C. E.; Baumann, E.; Boileau, E.; Stanimirovic, D. Multiplexed Evaluation of Serum and CSF Pharmacokinetics of Brain-Targeting Single-Domain Antibodies Using a NanoLC-SRM-ILIS Method. *Mol. Pharm.* **2013**, *10* (5), 1542–1556.

(27) Thompson, P.; Fleming, R.; Bezabeh, B.; Huang, F.; Mao, S.; Chen, C.; Harper, J.; Zhong, H.; Gao, X.; Yu, X.-Q.; Hinrichs, M. J.; Reed, M.; Kamal, A.; Strout, P.;

Cho, S.; Woods, R.; Hollingsworth, R. E.; Dixit, R.; Wu, H.; Gao, C.; Dimasi, N. Rational Design, Biophysical and Biological Characterization of Site-Specific Antibody-Tubulysin Conjugates with Improved Stability, Efficacy and Pharmacokinetics. *J. Control. Release* **2016**, *236*, 100–116.

(28) Hargreaves, K. M.; Troullos, E. S.; Dionne, R. A.; Schmidt, E. A.; Schafer, S. C.; Joris, J. L. Bradykinin Is Increased during Acute and Chronic Inflammation: Therapeutic Implications. *Clin. Pharmacol. Ther.* **1988**, *44* (6), 613–621.

(29) Farrington, G. K.; Caram-Salas, N.; Haqqani, A. S.; Brunette, E.; Eldredge, J.; Pepinsky, B.; Antognetti, G.; Baumann, E.; Ding, W.; Garber, E.; Jiang, S.; Delaney, C.; Boileau, E.; Sisk, W. P.; Stanimirovic, D. B. A Novel Platform for Engineering Blood-Brain Barrier-Crossing Bispecific Biologics. *FASEB J.* **2014**, *28* (11), 4764–4778.

(30) Webster, C. I.; Caram-Salas, N.; Haqqani, A. S.; Thom, G.; Brown, L.; Rennie, K.; Yogi, A.; Costain, W.; Brunette, E.; Stanimirovic, D. B. Brain Penetration, Target Engagement, and Disposition of the Blood-Brain Barrier-Crossing Bispecific Antibody Antagonist of Metabotropic Glutamate Receptor Type 1. *FASEB J.* **2016**, *30* (5), 1927–1940.

(31) Xu, S.-L.; Li, J.; Zhang, J.-J.; Yu, L.-C. Antinociceptive Effects of Galanin in the Nucleus Accumbens of Rats. *Neurosci. Lett.* **2012**, *520* (1), 43–46.

(32) Robertson, C. R.; Flynn, S. P.; White, H. S.; Bulaj, G. Anticonvulsant Neuropeptides as Drug Leads for Neurological Diseases. *Nat. Prod. Rep.* **2011**, *28* (4), 741.

(33) Wang, D.; Ye, H. H.; Yu, L. C.; Lundeberg, T. Intra-Periaqueductal Grey Injection of Galanin Increases the Nociceptive Response Latency in Rats, an Effect Reversed by Naloxone. *Brain Res.* **1999**, *834* (1–2), 152–154.

(34) Pardridge, W. M.; Buciak, J. L.; Friden, P. M. Selective Transport of an Anti-Transferrin Receptor Antibody through the Blood-Brain Barrier in Vivo. *J. Pharmacol. Exp. Ther.* **1991**, *259* (1), 66–70.

(35) Sumbria, R. K.; Zhou, Q.-H.; Hui, E. K.-W.; Lu, J. Z.; Boado, R. J.; Pardridge, W. M. Pharmacokinetics and Brain Uptake of an IgG-TNF Decoy Receptor Fusion Protein Following Intravenous, Intraperitoneal, and Subcutaneous Administration in Mice. *Mol. Pharm.* **2013**, *10* (4), 1425–1431.

(36) Zhou, Q.-H.; Fu, A.; Boado, R. J.; Hui, E. K.-W.; Lu, J. Z.; Pardridge, W. M. Receptor-Mediated Abeta Amyloid Antibody Targeting to Alzheimer's Disease Mouse Brain. *Mol. Pharm.* **2011**, *8* (1), 280–285.

(37) Yu, Y. J.; Atwal, J. K.; Zhang, Y.; Tong, R. K.; Wildsmith, K. R.; Tan, C.; Bien-Ly, N.; Hersom, M.; Maloney, J. A.; Meilandt, W. J.; Bumbaca, D.; Gadkar, K.; Hoyte, K.; Luk, W.; Lu, Y.; Ernst, J. A.; Scearce-Levie, K.; Couch, J. A.; Dennis, M. S.; Watts, R. J. Therapeutic Bispecific Antibodies Cross the Blood-Brain Barrier in Nonhuman Primates. *Sci. Transl. Med.* **2014**, *6* (261), 261ra154.

(38) Nuttall, S. D. Overview and Discovery of IgNARs and Generation of VNARs. *Methods Mol. Biol.* **2012**, *911*, 27–36.

(39) Connor, J. R.; Fine, R. E. The Distribution of Transferrin Immunoreactivity in the Rat Central Nervous System. *Brain Res.* **1986**, *368* (2), 319–328.

(40) Ruparel, N. B.; Patwardhan, A. M.; Akopian, A. N.; Hargreaves, K. M. Homologous and Heterologous Desensitization of Capsaicin and Mustard Oil Responses Utilize Different Cellular Pathways in Nociceptors. *Pain* **2008**, *135* (3), 271–279.

(41) Couch, J. A.; Yu, Y. J.; Zhang, Y.; Tarrant, J. M.; Fuji, R. N.; Meilandt, W. J.; Solanoy, H.; Tong, R. K.; Hoyte, K.; Luk, W.; Lu, Y.; Gadkar, K.; Prabhu, S.; Ordonia, B. A.; Nguyen, Q.; Lin, Y.; Lin, Z.; Balazs, M.; Scearce-Levie, K.; Ernst, J. A.; Dennis, M. S.; Watts, R. J. Addressing Safety Liabilities of TfR Bispecific Antibodies That Cross the Blood-Brain Barrier. *Sci. Transl. Med.* **2013**, *5* (183), 183ra57, 1-12.

(42) Gadkar, K.; Yadav, D. B.; Zuchero, J. Y.; Couch, J. A.; Kanodia, J.; Kenrick, M. K.; Atwal, J. K.; Dennis, M. S.; Prabhu, S.; Watts, R. J.; Joseph, S. B.; Ramanujan, S. Mathematical PKPD and Safety Model of Bispecific TfR/BACE1 Antibodies for the Optimization of Antibody Uptake in Brain. *Eur. J. Pharm. Biopharm.* **2016**, *101*, 53–61.

(43) Kanodia, J.; Gadkar, K.; Bumbaca, D.; Zhang, Y.; Tong, R.; Luk, W.; Hoyte, K.; Lu, Y.; Wildsmith, K.; Couch, J.; Watts, R.; Dennis, M.; Ernst, J.; Scearce-Levie, K.; Atwal, J.; Ramanujan, S.; Joseph, S. Prospective Design of Anti-Transferrin Receptor Bispecific Antibodies for Optimal Delivery into the Human Brain. *CPT Pharmacometrics Syst. Pharmacol.* **2016**, *5* (5), 283–291.

Tables

Table 1. Kinetic parameters for OX26 variants binding rTfR. Parameters were determined using an Octet assay where the IgG is immobilized and rTfR is in solution. Data were generated using a 1:1 binding model and are the mean of two replicate experiments.

Variant	k_{on} ($M^{-1}s^{-1}$)	k_{off} (s^{-1})	K_D (nM)
OX26	1.5×10^4	9.0×10^{-5}	5.0 ± 2
$OX26_{76}$	1.4×10^4	1.1×10^{-3}	76 ± 10
$OX26_{108}$	1.6×10^4	1.9×10^{-3}	108 ± 30
$OX26_{174}$	5.4×10^3	1.0×10^{-3}	174 ± 43

Table 2. Mean (%CV of the estimate) pharmacokinetic and brain distribution parameter estimates following intravenous administration of OX26 variants or NiP228 to naive rats. Parameters were derived using a model fitting all individual data points (6 animals per each time point). Estimates for all variants except $OX26_6$, which demonstrated a mono-exponential decay, were obtained using a two-compartment model with distinct distribution and elimination phases.

Parameter [a]	Unit	OX-26_5	OX-26_{76}	OX-26_{108}	OX-26_{174}	NiP228
Plasma Pharmacokinetics Parameters						
CL	mL/hr/kg	6.1 (7.0)	5.4 (5.6)	3.4 (13)	2.6 (16)	1.7 (41)
CL_D	mL/hr/kg	na	6.6 (15)	0.8 (11)	11 (14)	16 (42)
V_1	mL/kg	53 (8.2)	46 (11)	33 (10)	49 (9.3)	44 (9.3)
V_2	mL/kg	na	94 (19)	46 (111)	140 (23)	73 (36)
$t_{1/2\beta}$	hr	6 .1 (2.3) [b]	26 (16)	52 (93)	58 (31)	49 (58)
AUC_{plasma}	nmol*hr/L	22.7 (7)	25.8 (6)	36.1 (19)	54.4 (16)	81.2 (41)
Brain Pharmacokinetics Parameters						
$CL_{up,brain}$	µL/hr/kg	0.03 (13)	2.06 (9)	1.16 (7)	0.90 (7)	0.05 (14)
$CL_{out,brain}$	µL/hr/kg	180 (25)	121 (20)	244 (13)	336 (10)	321 (19)
$C_{max,brain}$	nM	0.064	3.35	3.10	1.12	0.094
AUC_{brain}	nmol/hr/mL	4.29	475	177	151	12.3
Brain Exposure						
AUC_{brain} / AUC_{plasma}	%	0.02	1.84	0.47	0.28	0.02

[a] *CL: Total body clearance. CL_D: Distribution clearance. V_1: Volume of distribution of central compartment. V_2: Volume of distribution of peripheral compartment. $t_{1/2\beta}$: Elimination half-life. $CL_{up,brain}$: Brain uptake clearance. $CL_{out,brain}$: Brain to serum clearance. AUC: Area under the concentration-time curve. $C_{max,brain}$: Predicted maximum concentration in brain.*

[b] For OX-26_5, terminal half-life derived from a monoexponential decay of serum concentrations vs time.

Table 3. CSF concentration-time profiles in rat following an equimolar intravenous bolus dose of 26.8 nmol/kg of OX26 variants, A20.1 or NIP228 to naive rats. Maximum observed CSF concentration reported as mean ± sd (n=3).

TfR variant or A20.1mFc	$AUC_{CSF,0\text{-}96}$ **(nmol*h/L)**	AUC_{CSF} / AUC_{Serum} **(%)**	CSF_{max} **(nM)**
$OX26_5$	84	0.38	1.76 ± 0.30
A20.1mFc	21	0.09	0.65 ± 0.04
$OX26_{76}$	146	0.55	3.10 ± 0.21
A20.1mFc	14	0.06	0.53 ± 0.12
$OX26_{108}$	133	0.66	2.84 ± 0.15
A20.1mFc	31	0.15	0.67 ± 0.48
$OX26_{174}$	40	0.18	0.73 ± 0.09
A20.1mFc	21	0.09	0.47 ± 0.02
NiP228	31	0.13	0.76 ± 0.42
A20.1mFc	24	0.11	0.57 ± 0.04

Table 4. Summary of reversal of thermal hyperalgesia in the Hargreaves model. $OX26_5$, $OX26_{76}$, $OX26_{108}$, $OX26_{174}$ and NiP-228 were administered at indicated doses by intravenous route. The percent reversal of thermal hyperalgesia at peak response, time to peak response, the duration of the response, and the AUC of the response are shown as means ± sem for 3-6 animals in each group.

TfR variant	Dose [nmol/kg]	% of reversal	Time to Emax (min)	Duration (min)	AUC (s x min)
$OX26_5$	10	10.2 ± 3.8	92.8 ± 7.4	10.1 ± 6.5	284 ± 95
$OX26_5$	30	69.2 ± 5.0	107.1 ± 10.7	150.0 ± 10.7	976 ± 87*
$OX26_{76}$	10	58.9 ± 5.7	101.7 ± 7.8	117.9 ± 16.7	745 ± 117*#
$OX26_{108}$	10	53.6 ± 6.0	92.8 ± 3.9	108.9 ± 10.3	663 ± 110*#
$OX26_{174}$	10	23.7 ± 5.6	88.3 ± 3.6	22.7 ± 9.8	306 ± 72
NiP-228	10	8.3 ± 1.7	102.6 ± 11.7	4.0 ± 3.4	167 ± 25

Asterisks indicate a significant difference in AUC ($P<0.01$; ANOVA) compared to NiP-228; number signs indicate a significant difference ($P<0.01$; ANOVA) from the same dose of $OX26_5$

Figure Captions

Figure 1. A) Observed and predicted serum (upper panels) and brain (lower panels) concentrations versus time plots for OX26 variants and NIP228. Animals were administered 20 mg/kg iv. of OX26 variants or NIP228, serum and brain levels were measured by ELISA, and serum and brain concentrations-time profiles were analyzed using WinNonlin software (Version 7.0, Pharsight Corporation, Mountain View, CA, USA) as described in Material and Methods. Detailed PK parameters are shown in Table 2. B) Cerebrospinal fluid (CSF) exposure of OX26 affinity variants and control antibodies A20.1mFc and NiP228. Animals were co-injected iv an equimolar dose (30 nmol/kg) of test antibody (OX26 variant or NiP228) and control antibody (A20.1mFc) via a tail vein, and CSF levels were measured at indicated time points over 96 h using multiplexed SRM technique as described in Material and Methods. Results are shown as means ± SD for 3 animals in each time point. Apparent CSF exposure (AUC_{CSF}) from each paired antibody administration is shown in Table 3.

Figure 2. Detection of intravenously injected OX26 variants in rat brain sections by immunofluorescence. Animals received 7 mg/kg iv. of either control antibody NiP228 (A), $OX26_5$ (C&E) or $OX26_{76}$ (D&F) and were perfused 4 h after injections. The antibodies were immuno-detected using biotinylated goat anti-human IgG followed by streptavidin-Cy3, shown as red staining. The sections were then counter-stained for the neuronal marker NeuN (green) and nuclear stain Hoechst (blue). Red channel only and corresponding composite images were shown in pairs. Image in B is a control where only secondary antibody was used. Fluorescent

micrographs of frontal cortex (left column of paired images) and parietal cortex (right column of paired images) are shown. In animals injected with $OX26_5$, both frontal cortex (C1-C2) and parietal cortex (E1-E2) show immunoreactivity in blood vessels only. Two separate sections of both frontal cortex (D1-D4) and parietal cortex (F1-F4) of animals injected with $OX26_{76}$ are shown to illustrate immuno-positive neurons (marked with stars).

Figure 3. Inhibition of thermal hyperalgesia in rat after systemic administration of OX26 affinity variants or control antibody NiP-228 conjugated to neuropeptide galanin. The potency of all antibodies was compared at 10 nmol/kg dose as described in Material and Methods. A) Paw withdrawal latency of inflamed paw in response to a thermal stimulus measured after a single intravenous bolus injection of NiP228, $OX26_5$, $OX26_{76}$, $OX26_{108}$ or $OX26_{174}$. Latency was measured at 15 min intervals over a 4-h period. Data are shown as means ± sem for 3–6 separate animals in each group. The control paw shows latency of 20 s or more, whereas inflamed paw in animals receiving PBS shows latency of ~5 s. The latency of paw withrawal was prolonged by $OX26_{76}$-Gal and $OX26_{108}$-Gal, while $OX26_5$-Gal and $OX26_{174}$-Gal produced marginal response (detailed parameters of the response and statistics are shown in Table 4). B) Serum and CSF levels of variants at the end of experiment in A (at 240 min) are measured by multiplexed SRM. Significant increase in CSF levels was measured for $OX26_{76}$-Gal and $OX26_{108}$-Gal conjugates compared to control antibody NiP228-Gal conjugate. The levels of $OX26_6$ dosed at 30 nmol/kg were also included (see corresponding potency data in Table 4).

Figure 1

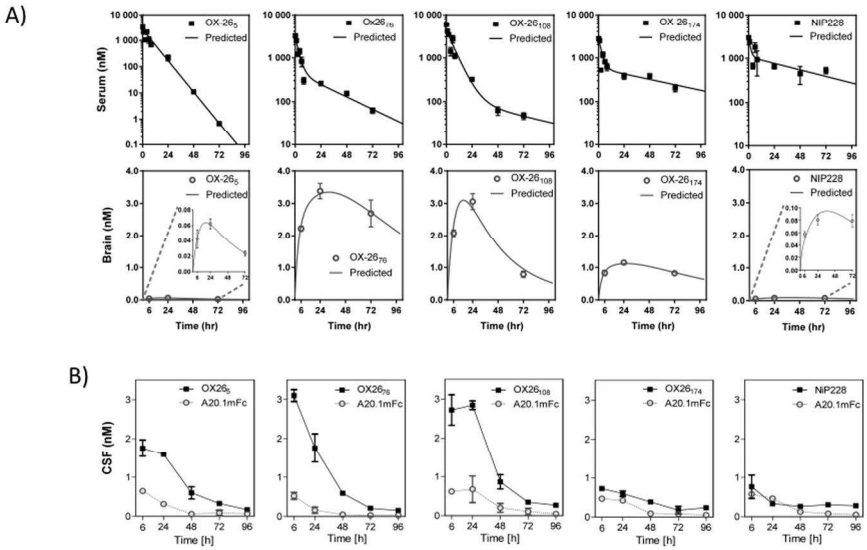

Figure 1

170x127mm (300 x 300 DPI)

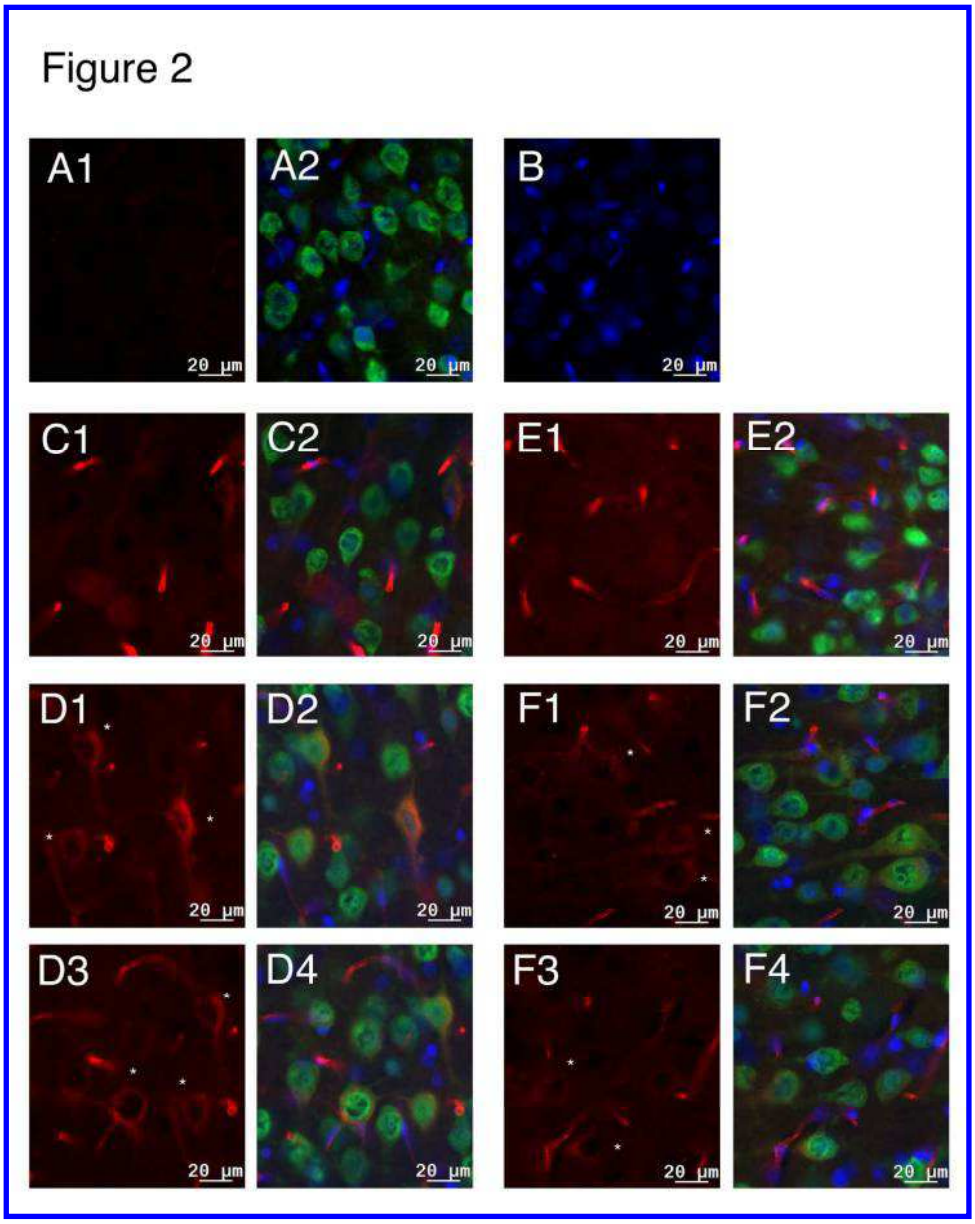

Figure 2

194x244mm (300 x 300 DPI)

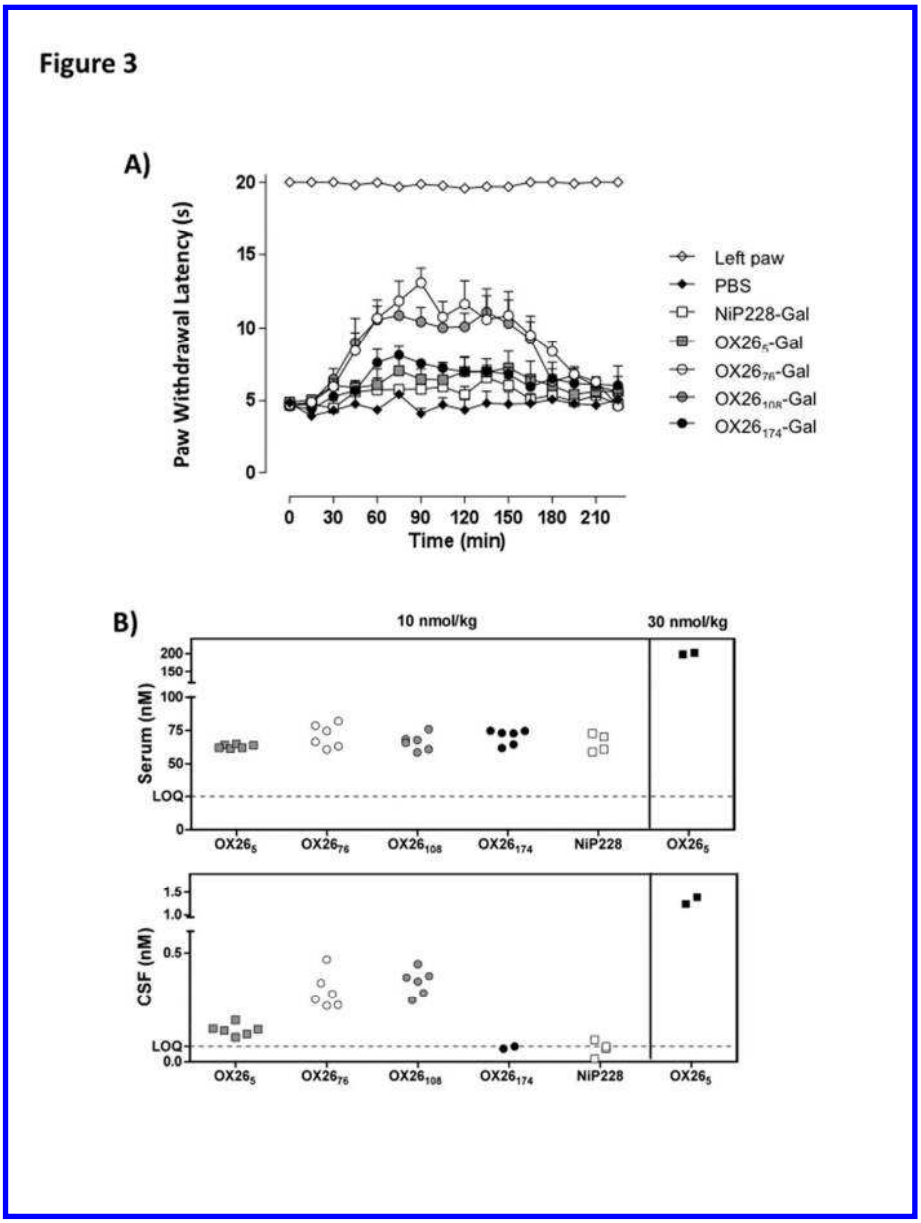

Figure 3

88x118mm (300 x 300 DPI)

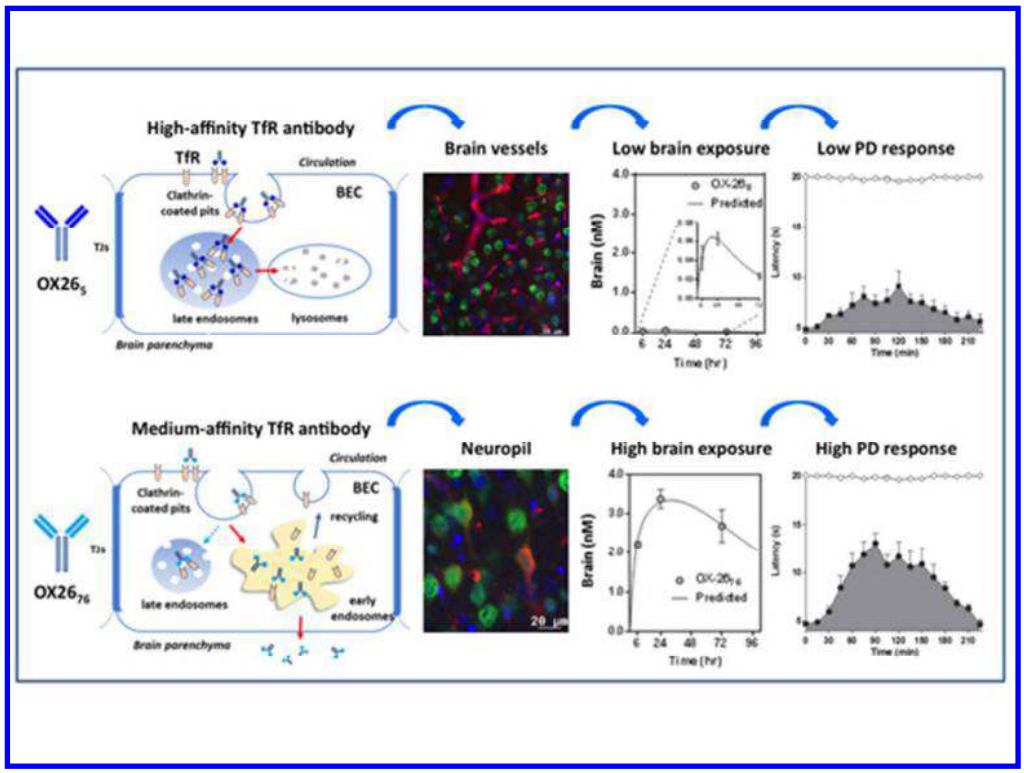

Table of contents graphic

48x35mm (300 x 300 DPI)